Pure appl. geophys. 166 (2009) 353–374
0033–4553/09/030353–22
DOI 10.1007/s00024-009-0451-z

Pure and Applied Geophysics

Dipping-interface Mapping Using Mode-separated Rayleigh Waves

YINHE LUO,[1] JIANGHAI XIA,[2] YIXIAN XU,[3] CHONG ZENG,[2] RICHARD D. MILLER,[2] and QINGSHENG LIU[1]

Abstract—Multichannel analysis of surface waves (MASW) method is a non-invasive geophysical technique that uses the dispersive characteristic of Rayleigh waves to estimate a vertical shear (S)-wave velocity profile. A pseudo-2D S-wave velocity section is constructed by aligning 1D S-wave velocity profiles at the midpoint of each receiver spread that are contoured using a spatial interpolation scheme. The horizontal resolution of the section is therefore most influenced by the receiver spread length and the source interval. Based on the assumption that a dipping-layer model can be regarded as stepped flat layers, high-resolution linear Radon transform (LRT) has been proposed to image Rayleigh-wave dispersive energy and separate modes of Rayleigh waves from a multichannel record. With the mode-separation technique, therefore, a dispersion curve that possesses satisfactory accuracy can be calculated using a pair of consecutive traces within a mode-separated shot gather. In this study, using synthetic models containing a dipping layer with a slope of 5, 10, 15, 20, or 30 degrees and a real-world example, we assess the ability of using high-resolution LRT to image and separate fundamental-mode Rayleigh waves from raw surface-wave data and accuracy of dispersion curves generated by a pair of consecutive traces within a mode-separated shot gather. Results of synthetic and real-world examples demonstrate that a dipping interface with a slope smaller than 15 degrees can be successfully mapped by separated fundamental waves using high-resolution LRT.

Key words: Rayleigh waves, pseudo-2D S-wave velocity section, high-resolution linear Radon transform, mode separation, dipping layer.

1. Introduction

Multichannel analysis of surface waves (MASW) method is a non-invasive geophysical technique that uses the dispersive characteristic of Rayleigh waves to estimate the vertical shear (S)-wave velocity (SONG *et al.*, 1989; XIA *et al.*, 1999, 2002a, b, 2006; PARK *et al.*, 1999; CALDERÓN-MACÍAS and LUKE, 2007; LUO *et al.*, 2007). A pseudo-2D S-wave velocity section is constructed by aligning 1D models at the midpoint of each receiver spread and using a spatial interpolation scheme (MILLER *et al.*, 1999; XIA *et al.*, 2005; LUO *et al.*,

[1] Institute of Geophysics and Geomatics, China University of Geosciences, Wuhan, Hubei 430074, China. E-mail: yluo@kgs.ku.edu; luoyinhe@cug.edu.cn

[2] Kansas Geological Survey, The University of Kansas, 1930 Constant Avenue, Lawrence, Kansas 66047-3724, USA.

[3] State Key Laboratory of Geological Processes and Mineral Resources, Institute of Geophysics and Geomatics, China University of Geosciences, Wuhan, Hubei 430074, China.

2008a). The horizontal resolution of the inverted S-wave velocity section with the MASW technique is most influenced by receiver-spread length (the distance between the first and last receivers) and acquisition interval (the distance covered by the same source-receiver configuration) (Xia *et al.*, 2005; Luo *et al.*, 2008a, b). The receiver-spread length sets the theoretical lower limit. Any Vs structure whose lateral dimension is shorter than the receiver-spread length will not be properly resolved in the final Vs section. An acquisition interval shorter than the spread length will not improve this limitation because spatial smearing has already been introduced by the receiver spread (Park, 2005). Xia *et al.* (2005) discussed the resolving power of the MASW technique and resolution of S-wave velocity and presented a lateral unblurring processing by generalized inversion to increase horizontal resolution of a pseudo-2D S-wave velocity section.

The most direct and effective way to improve the horizontal resolution of inverted S-wave velocity is to extract accurate dispersion curves from a record with a short geophone spread (Xia et al., 2005). Based on the (stepped-flat-layer) assumption that a dipping-layer model can be regarded as stepped flat layers (Kuo and Thompson, 1963), Guo and Liu (1999), Liu *et al.* (2003), and Hayashi and Suzuki (2004) used a cross-correlation method to calculate dispersion curves, choosing a pair of consecutive receivers in the multichannel record. This method possesses high potential to improve the horizontal resolution of pseudo-2D sections without acquiring redundant data. Similar to SASW, this method is sensitive to noise in data and unrealistic results will be generated if the data have a low signal-to-noise (S/N) ratio. Luo *et al.* (2008a) used a combined method of cross-correlation and phase-shift scanning to calculate the dispersion curve, which also uses a pair of consecutive traces in a multichannel record. The combined method can effectively enhance the ability of random-noise immunity but fails to cope with interferences of body waves and high-mode Rayleigh waves.

The main challenge of using a pair of consecutive traces to calculate the dispersion curve is to recognize the fundamental-mode Rayleigh waves from raw surface-wave data because the fundamental mode is easily contaminated by high modes or body waves. Bodet *et al.* (2005) carried out laser-doppler physical modeling to determine limitations of multichannel analysis of surface waves and presented that a layer dip of only a few degrees can significantly bias the surface-wave inversion. However, a dispersive image in the frequency-phase velocity (*f*-*v*) domain that is generated from multichannel surface-wave data makes it much easier to recognize the fundamental-mode Rayleigh waves, high-mode Rayleigh waves, and body waves, which provides a foundation to separate fundamental-mode Rayleigh waves by a proper dispersive-imaging algorithm. Four algorithms for dispersive-imaging computation, based on F-K spectrum (e.g., Yilmaz, 1987), tau-p transform (McMechan and Yedlin, 1981), phase shift (Park *et al.*, 1998), and slant stacking (Xia *et al.*, 2007a), are kinds of standard discretized linear Radon transform (LRT). Because standard LRT suffers from typical problems of loss of resolution and aliasing that arise as a consequence of incomplete information, such as limited aperture and discretization (Trad *et al.*, 2002, 2003), it is difficult to separate fundamental-mode Rayleigh waves from raw surface-wave data with a standard LRT.

An appealing solution to efficiently image dispersive energy and separate multimode Rayleigh waves can be obtained by high-resolution LRT (Sacchi and Ulrych, 1995; Schonewille and Duijndam, 2001; Trad *et al*., 2002, 2003; Ethan and Matthias, 2006). Because high-resolution LRT attenuates aliasing and improves resolution to some degree by use of a sparseness inversion technique, it can effectively preserve amplitude and angle information and image dispersion energy with high resolution. Based on the stepped-flat-layer assumption, Luo *et al*. (2008c, in review) proposed to image Rayleigh-wave dispersive energy and separate multimode Rayleigh waves from a multichannel record by high-resolution LRT. They used a pair of consecutive traces within the mode-separated shot gather to calculate a dispersion curve and achieved satisfactory results with synthetic and real-world data.

In many real-world applications, S-wave velocities vary violently. Great effort should be made to evaluate the validity of the stepped-flat-layer assumption. In this study, we use synthetic models containing a dipping layer with a slope of 5, 10, 15, 20, or 30 degrees and a real-world example to assess the ability of using high-resolution LRT to image and separate fundamental-mode Rayleigh waves from raw surface-wave data and accuracy of dispersion curves generated by a pair of consecutive traces within a mode-separated shot gather.

2. *High-resolution Linear Radon Transform*

The linear Radon transform (LRT) is a plane-wave decomposition accomplished by summing over amplitudes after applying a linear moveout to data (Yilmaz, 1987). The forward LRT can be written in matrix form as

$$\mathbf{d} = \mathbf{L}\mathbf{m} \tag{1}$$

and the adjoint transformation,

$$\mathbf{m}_{adj} = \mathbf{L}^T\mathbf{d}, \tag{2}$$

where $\mathbf{L} = e^{i2\pi fpx}$ is the forward LRT operator, $\mathbf{d}$ and $\mathbf{m}$ represent the shot gather and Radon panel (the estimated data in frequency-slowness domain), $\mathbf{m}_{adj}$ denotes a low-resolution Radon panel using the transpose or adjoint operator $\mathbf{L}^T$. It is clear that because $\mathbf{L}$ is not a unitary operator, $\mathbf{L}^T$ does not define the inverse operator. It is hard to achieve high-resolution images of dispersion energy from standard LRT because they suffer from the loss of resolution and aliasing arising as a consequence of incomplete information, including limited aperture and discretization (Trad *et al*., 2003).

Sparsity constraint should be considered when finding the model $\mathbf{m}$ that best fits the data while minimizing the number of model-space parameters that are necessary to represent the data in the Radon domain. The model $\mathbf{m}$ can be defined by solving the following equation (Trad *et al*., 2002, 2003):

$$(\mathbf{W}_m^{-T}\mathbf{L}^T\mathbf{W}_d^T\mathbf{W}_d\mathbf{L}\mathbf{W}_m^{-1} + \lambda\mathbf{I})\mathbf{W}_m\mathbf{m} = \mathbf{W}_m^{-T}\mathbf{L}^T\mathbf{W}_d^T\mathbf{W}_d\mathbf{d}, \quad (3)$$

where $\mathbf{I}$ denotes the identity matrix; $\mathbf{W}_d$ is a matrix of data weights; $\mathbf{W}_m$ is a matrix of model weights that plays an extremely important role in the design of high-resolution Radon operators, for example, resolution and smoothness; $\mathbf{W}_m^{-T}$ is the transpose matrix of $\mathbf{W}_m^{-1}$; and λ maintains balance between data misfit and model constraints. Formula (3) can be solved very efficiently by CG algorithm, and details of the strategy can be found in many sources (SACCHI and PORSANI, 1999; TRAD *et al.*, 2002; 2003).

It is straightforward to image dispersive energy by high-resolution LRT (LUO *et al.*, 2008c). First, the shot gather is transformed along time into the frequency domain. Then the high-resolution LRT is completed for each frequency slice, and the Radon panel is transformed from the frequency-slowness domain to the frequency-velocity domain using a linear-interpolation operation. Rayleigh-wave mode separation by high-resolution LRT needs three more steps: selecting modes, transforming different modes back to the *t-x* domain along the time coordinate, and imaging different-mode dispersive energy in the velocity-frequency domain (LUO *et al.*, in review). In summary, the processing flow of generating a 2D S-wave velocity section is as follows:

1. Imaging dispersive energy by high-resolution LRT,
2. Separating fundamental-mode Rayleigh waves manually and muting the rest in the *f-v* domain, and performing forward high-resolution LRT to form a record that only contains the fundamental mode,
3. Calculating dispersion curves by a pair of consecutive traces with the following formula

$$v_R(f) = \frac{2\pi f \Delta x}{\Delta\phi}, \quad (4)$$

where $v_R(f)$ is the phase velocity of a Rayleigh wave at the frequency f, $\Delta\phi(f)$ is the phase difference, and Δx is the distance between a pair of consecutive traces, and

4. Estimating S-wave velocity sections by inverting each dispersion curve (XIA *et al.*, 1999).

3. Synthetic Examples

In this section, a synthetic shot gather (the vertical component) due to a dipping layer with a slope of 5, 10, 15, 20, or 30 degrees was computed by a finite-difference method (XU *et al.*, 2007). The source is a point source on the surface. We use these data to assess the ability of using high-resolution LRT to image and separate fundamental-mode

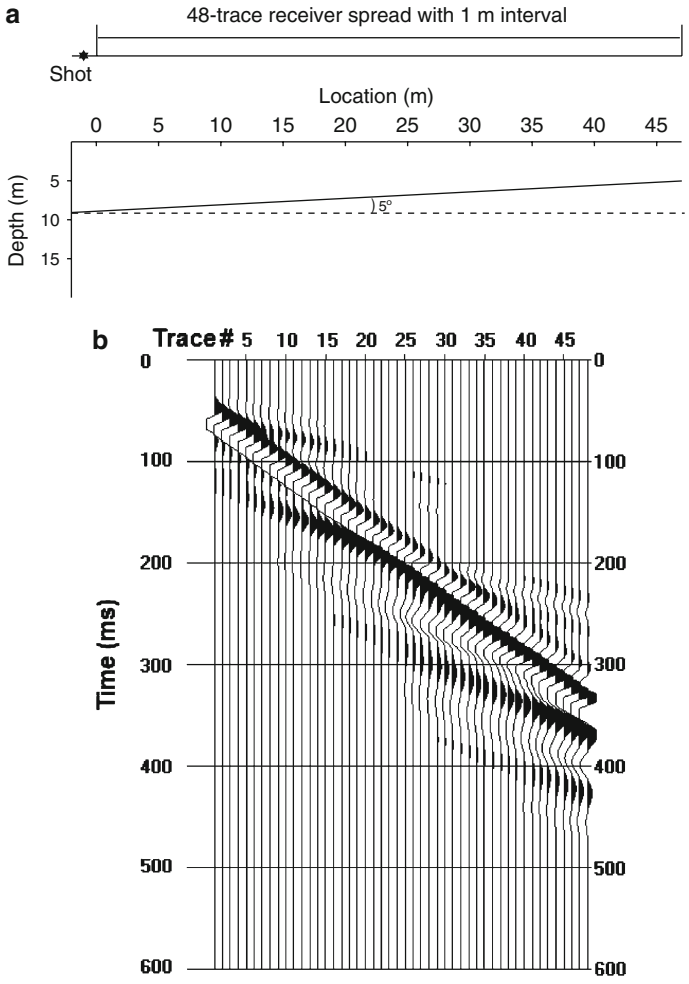

Figure 1
(a) A 5-degree slope model. (b) 48-channel synthetic vertical-component data computed by finite-difference method (Xu *et al*., 2007).

Rayleigh waves from raw surface-wave data and accuracy of dispersion curves generated by a pair of consecutive traces within a mode-separated shot gather.

3.1. A 5-degree Slope Model

This model consists of a 5-degree slope layer with Vp = 800 m/s, Vs = 200 m/s, and $\rho = 2000$ kg/m^3, over the half-space where Vp = 1200 m/s, Vs = 400 m/s, and $\rho = 2000$ kg/m^3 (Fig. 1a). In the finite-difference method, the spatial-grid size was 0.2 m with time step of 0.01 ms, source is described by the first-order derivative of

Gaussian function $t\cdot\exp(-at^2)$with controlling parameter $a = 3000$, and the minimum shot-geophone offset was selected as 1 m with a 1 m geophone interval. A 48-channel record was simulated (Fig. 1b).

Spectrum analysis showed the data (Fig. 1b) possess a dominant frequency for Rayleigh waves of 20 Hz with a frequency band of 10 Hz to 60 Hz. We obtained the image in the *f-v* domain by high-resolution LRT (Fig. 2a). We selected fundamental mode in the *f-v* domain (Fig. 2a) and applied the forward Radon transform to generate data in the *t-x* domain that contain only fundamental-mode Rayleigh waves (Fig. 2b). Forty-seven dispersion curves were calculated by a pair of consecutive traces within the mode-separated shot gather using formula (4). Phase-velocity section is generated by interpolation of forty-seven dispersion curves (Fig. 3a).

The phase velocity section (Fig. 3a) clearly reveals a slope along the survey direction. According to one-half-wavelength estimations (Sanchez-Salinero *et al.*, 1987) and different wavelengths carrying geological information at different depths (Babushka and Cara, 1991), we can roughly interpret the phase velocity section as a slope variation from 8 m to 4.5 m, deeming 210 m/s phase velocity as a threshold value between the dipping layer and the half space.

The stepped-flat-layer assumption allows us to generate the phase velocity section by interpolation of forty-seven dispersion curves calculated by Knopoff method (Schwab and Knopoff, 1972). We used the analytical results (Fig. 3b) to assess the accuracy of the phase velocity section (Fig. 3a). We notice that (1) the overall relative errors are about 3% with the largest relative error being 5.8% (Fig. 3c). As a rule of thumb, therefore, inverted S-wave velocities will possess over 95% accuracy (Xia *et al.*, 1999, 2002a); (2) The phase-velocity section (Fig. 3a) indicates a relatively higher phase velocity compared with the analytical results in the near offset range and a relatively lower phase velocity compared with the analytical results (< 5%) in the far offset range, which may due to near-field effects (e.g., non-plane wave propagation and body-wave energy) and artifacts of the finite-difference approximation (Xu *et al.*, 2007; Xia *et al.*, 2007b).

3.2. A 10-degree Slope Model

This model consists of a 10-degree slope layer (Fig. 4a), and the other parameters are the same as those for the 5-degree slope model. A 48-channel record (Fig. 4b) was simulated by a finite-difference method (Xu *et al.*, 2007). The grid size, time step, and time function were the same as used in the 5-degree slope model. We obtained the image in the *f-v* domain by high-resolution LRT (Fig. 5a). We selected fundamental mode in the *f-v* domain (Fig. 5a) and applied the forward Radon transform to generate data in the *t-x* domain that contains only fundamental-mode Rayleigh waves (Fig. 5b). Forty-seven dispersion curves were calculated by a pair of consecutive traces within the mode-separated shot gather using formula (4). Phase-velocity section is generated by interpolation of 47 dispersion curves (Fig. 6a).

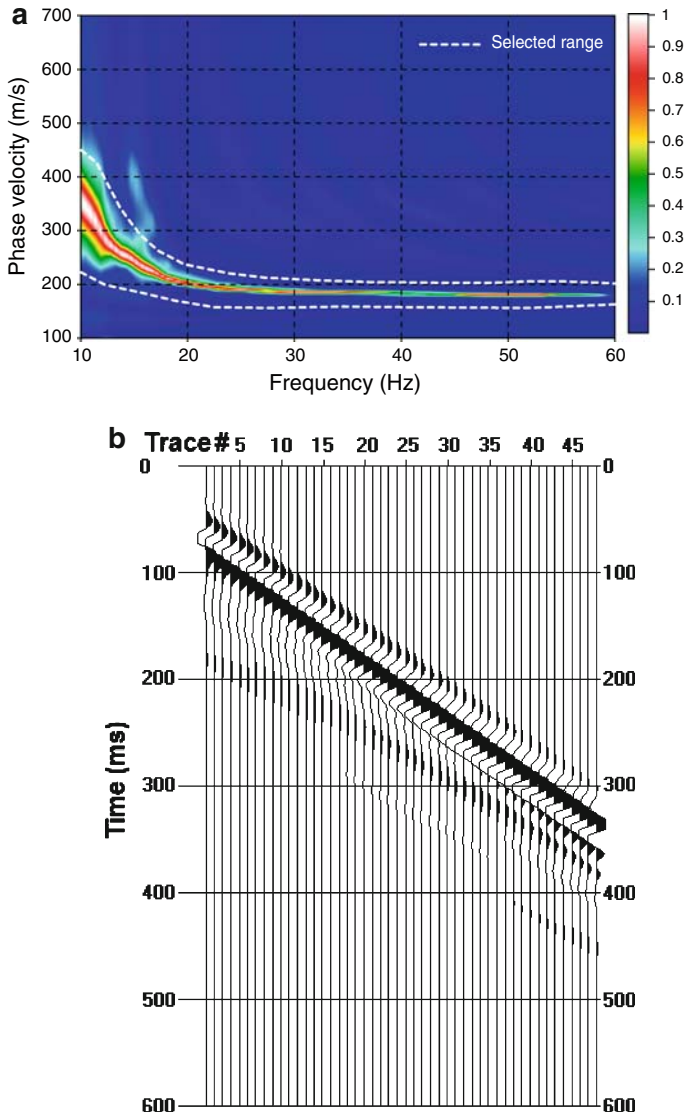

Figure 2
(a) An image of dispersive energy in the *f-v* domain generated by high-resolution LRT and the selected fundamental mode within dash lines. (b) A regenerated fundamental-mode shot gather.

The phase-velocity section (Fig. 6a) reveals a slope along the survey direction. According to one-half-wavelength estimations (Sanchez-Salinero *et al.*, 1987) and different wavelengths carrying geological information at different depths (Babushka and Cara, 1991), we can roughly interpret the phase velocity section as a slope variation from

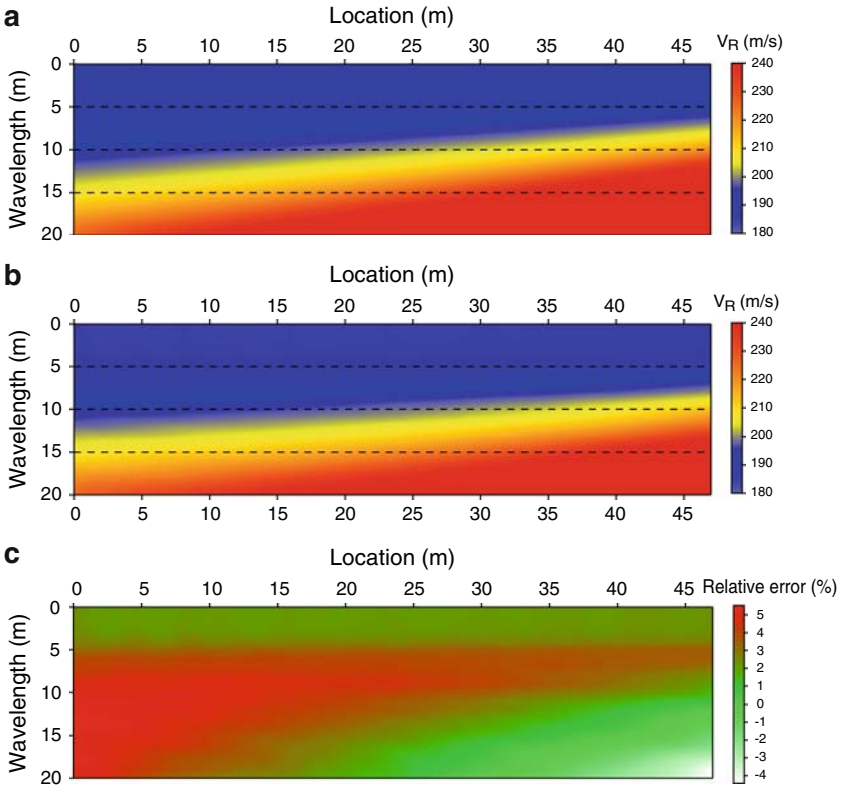

Figure 3

(a) Phase velocity section generated by interpolation of a series of dispersion curves calculated by a pair of consecutive traces in the fundamental-mode shot gather. (b) Phase-velocity sections generated by interpolation of a series of dispersion curves calculated by the Knopoff method (SCHWAB and KNOPOFF, 1972). (c) Relative errors in (a).

12 m to 4 m, deeming 210 m/s phase velocity as a threshold value between the dipping layer and half space.

We used the analytical results (Fig. 6b) section by interpolation of 47 dispersion curves calculated by the Knopoff method (SCHWAB and KNOPOFF, 1972) to assess the accuracy of the phase-velocity section (Fig. 6a). The overall relative errors are about 5% with the largest relative error being 7.9% (Fig. 6c). As a rule of thumb, therefore, inverted S-wave velocities will possess over 90% accuracy (XIA *et al.*, 1999, 2002a).

3.3. A 15-degree Slope Model

This model consists of a 15-degree slope layer (Fig. 7a) and the parameters are the same as those for the 5-degree slope model. A 48-channel record (Fig. 7b) was simulated by a finite-difference method (XU *et al.*, 2007). The grid size, time step, and time function

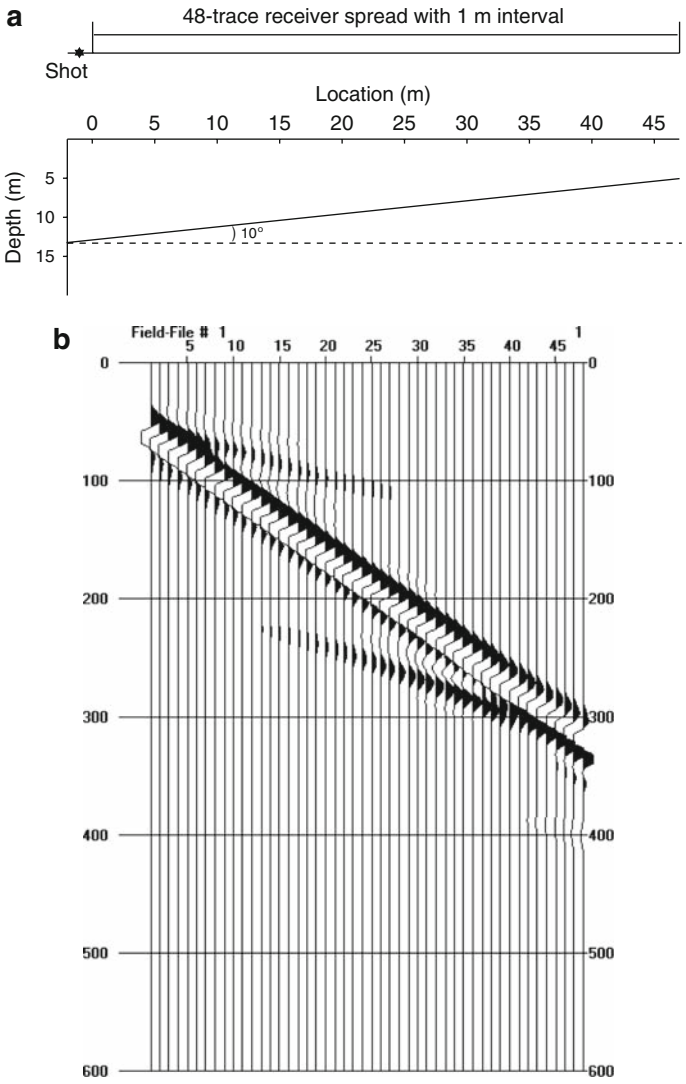

Figure 4
(a) A 10-degree slope model. (b) 48-channel synthetic vertical-component data computed by finite difference method (Xu *et al.*, 2007).

were the same as used in the 5-degree slope model. We obtained the image in the *f-v* domain by high-resolution LRT (Fig. 8a). We selected fundamental mode in the *f-v* domain (Fig. 8a) and applied the forward Radon transform to generate data in the *t-x* domain that contains only fundamental-mode Rayleigh waves (Fig. 8b). Forty-seven dispersion curves were calculated by a pair of consecutive traces within the mode-separated shot gather using formula (4). Phase-velocity section is generated by interpolation of 47 dispersion curves (Fig. 9a).

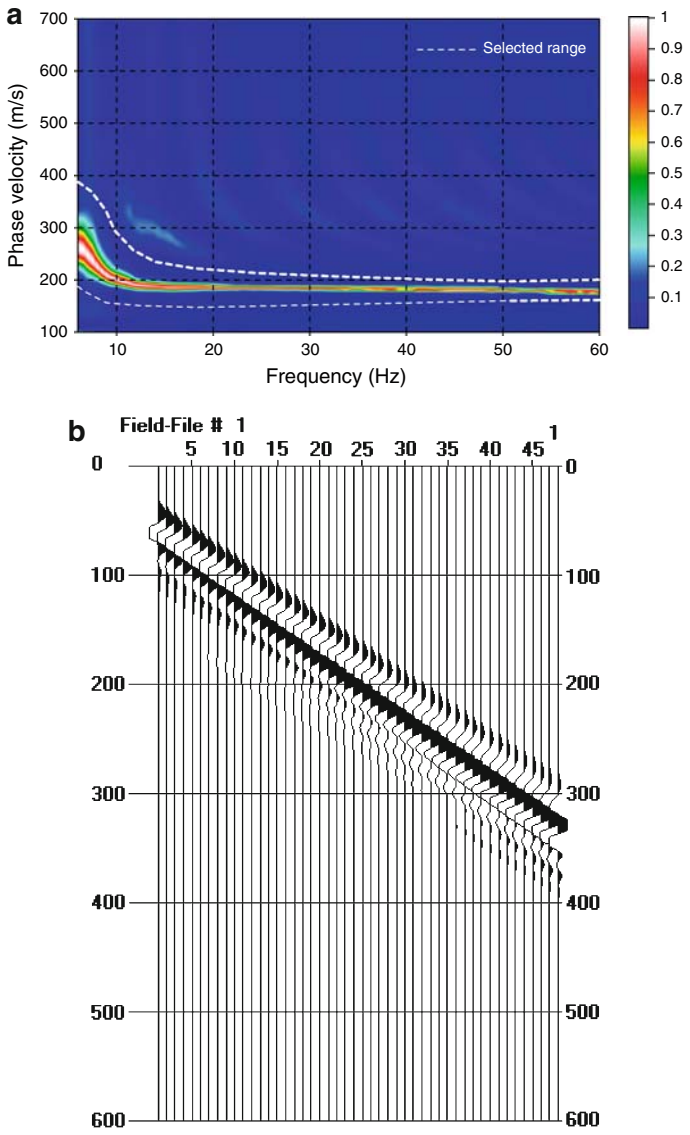

Figure 5
(a) An image of dispersive energy in the *f-v* domain generated by high-resolution LRT and the selected fundamental mode within dash lines. (b) A regenerated fundamental-mode shot gather.

We use the analytical results (Fig. 9b) section by interpolation of 47 dispersion curves calculated by Knopoff method (Schwab and Knopoff, 1972) to assess the accuracy of the phase-velocity section (Fig. 9a). The overall relative errors are about 12% with the largest relative error being 20% (Fig. 9c). It is impossible to correctly select the

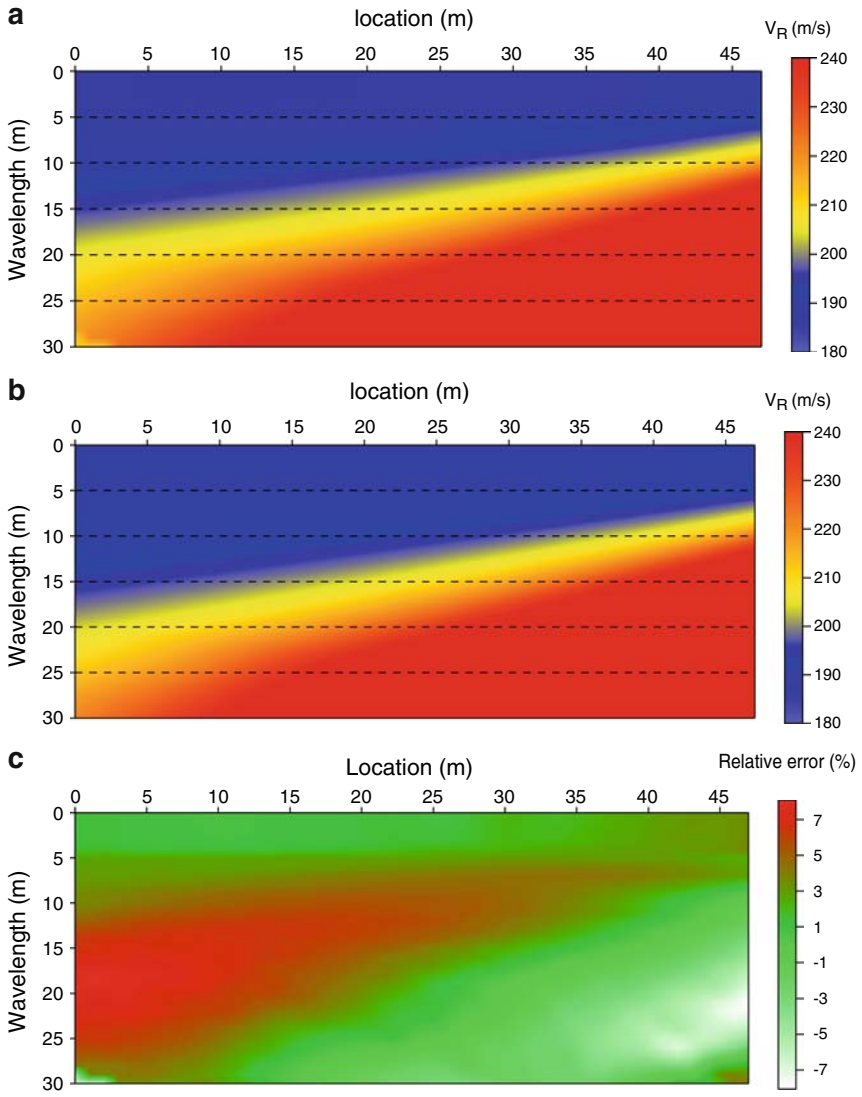

Figure 6

(a) Phase velocity section generated by interpolation of a series of dispersion curves calculated by a pair of consecutive traces in the fundamental-mode shot gather. (b) Phase-velocity sections generated by interpolation of a series of dispersion curves calculated by the Knopoff method (SCHWAB and KNOPOFF, 1972). (c) Relative errors in (a).

fundamental mode because the fundamental mode and higher modes interfere with each other. (Fig. 9d). In the selected range, the fundamental, first-, and part of second-mode Rayleigh waves of a two-layer model with a 17-m-thick top layer are included, while only part of the fundamental-mode Rayleigh waves of a two-layer model with a

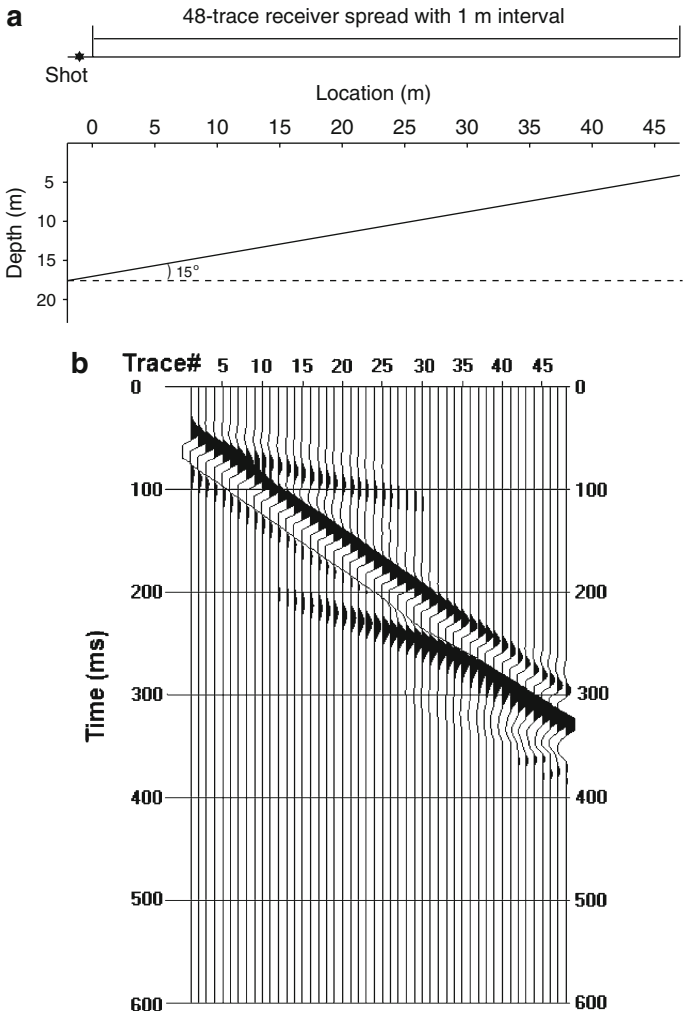

Figure 7
(a) A 15-degree slope model. (b) 48-channel synthetic vertical-component data computed by finite difference method (Xu *et al.*, 2007).

4-m-thick top layer are excluded (Fig. 9d), which results in higher phase velocities compared with the analytical results in the near offset range and lower phase velocities compared with the analytical results in the far offset range.

Results in the previous paragraphs show that properly separating fundamental-mode Rayleigh waves from multichannel surface-wave data is a key step for pseudo-2D S-wave velocity mapping with high horizontal resolution. For 5-degree and 10-degree models, we have successfully separated fundamental-mode Rayleigh waves from raw surface-wave data using high-resolution LRT and used a pair of consecutive traces within a

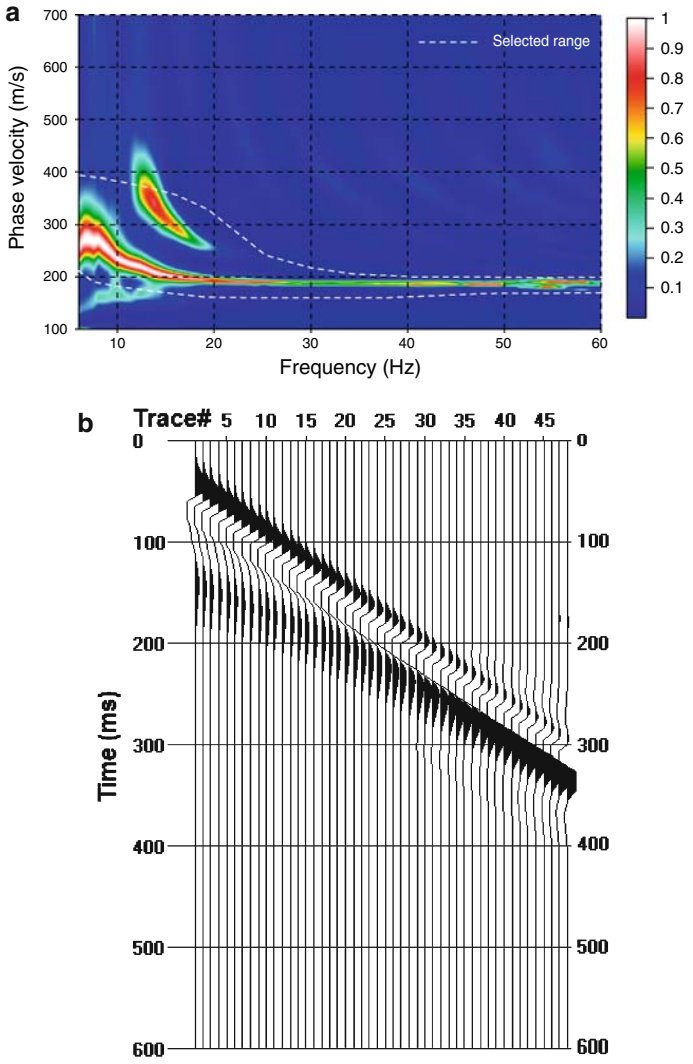

Figure 8
(a) An image of dispersive energy in the *f-v* domain generated by high-resolution LRT and the selected fundamental mode within dash lines. (b) A regenerated fundamental-mode shot gather.

mode-separated shot gather to calculate dispersion curves. For the 15-degree model, however, different modes of Rayleigh waves interfere with each other in the *f-v* domain so it is impossible to separate fundamental-mode Rayleigh waves from surface-wave data. Therefore, we are unable to generate dispersion curves with high horizontal resolution. Based on results of 20-degree and 30-degree dipping layers (Figs. 10a and 10b), we may conclude that the larger the dip angle of the slope in a model, the more severe the mode interference.

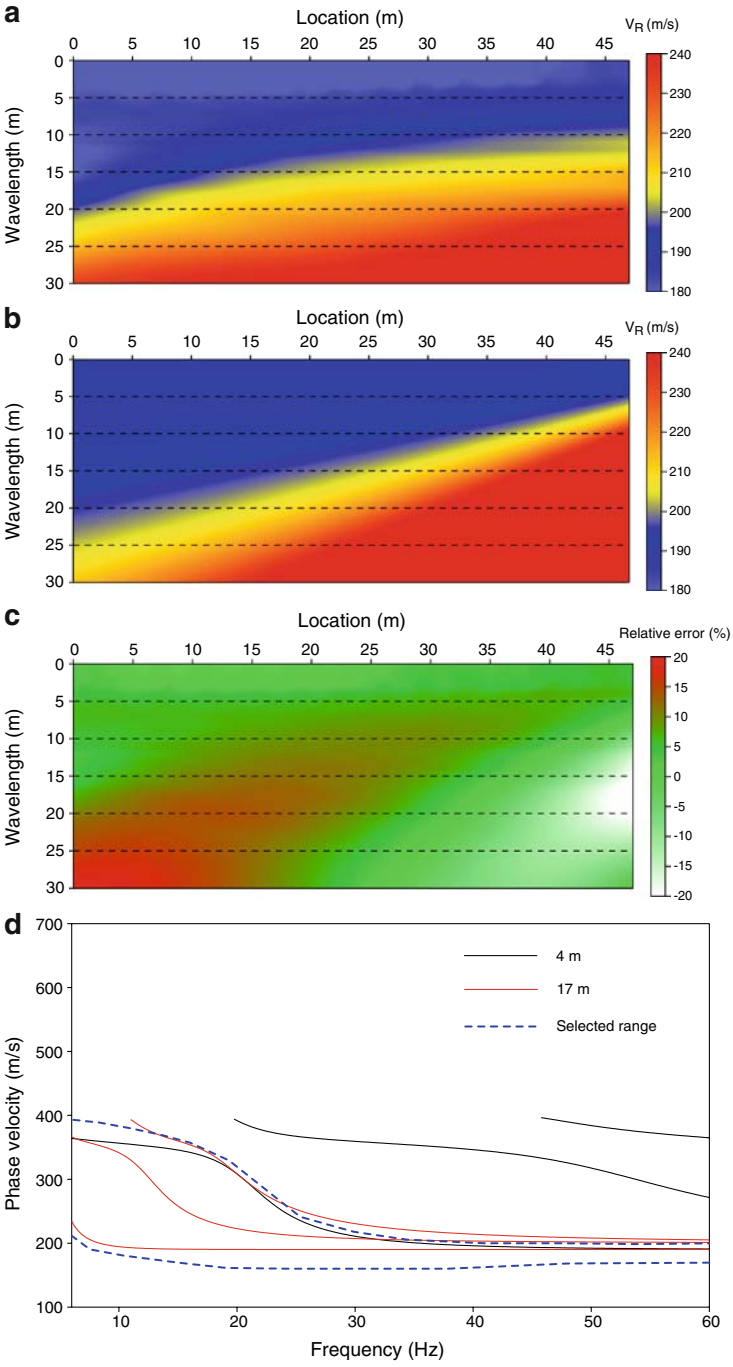
a
Location (m)
V_R (m/s)
Wavelength (m)
b
Location (m)
V_R (m/s)
Wavelength (m)
c
Location (m)
Relative error (%)
Wavelength (m)
d
Phase velocity (m/s)
Frequency (Hz)
4 m
17 m
Selected range

◀ Figure 9
(a) Phase-velocity section generated by interpolation of a series of dispersion curves calculated by a pair of consecutive traces in the fundamental-mode shot gather. (b) Phase-velocity sections generated by interpolation of a series of dispersion curves calculated by the Knopoff method (Schwab and Knopoff, 1972). (c) Relative errors in (a). (d) The fundamental-, first-, and second-mode theoretical dispersion curves and the selected fundamental-mode range in Figure 8a.

4. A Real-world Example

Real-world data were employed to assess the ability of using high-resolution LRT to image and separate fundamental-mode Rayleigh waves from raw surface-wave data and accuracy of dispersion curves generated by a pair of consecutive traces within a mode-separated shot gather. Thirty-six-channel surface-wave data were acquired at the campus of the China University of Geosciences, Wuhan, China, during the spring of 2007 using a Geometrics Strataview Seismograph and 4.5-Hz vertical-component geophones (Fig. 11a). The geophone interval was 0.5 m with a 6-m minimum source-to-receiver offset. The record length was 512 ms with a 0.5-ms sample interval. The source was a 5.4-kg hammer vertically impacting a 0.3-m by 0.3-m metal plate. With these geophones and acquisition geometry, dispersive energy was well developed and dominant in the recorded data (Fig. 11a). The object of the survey was to use surface-wave techniques to delineate the subsurface up to 8-m-depth.

Spectral analysis shows Rayleigh waves (Fig. 11a) possessing a dominant frequency around 50 Hz with a usable bandwidth from 15 Hz to 100 Hz. We obtained the image in the *f-v* domain by high-resolution LRT (Fig. 11b). The fundamental and first higher Rayleigh-wave energy levels are very close in the recorded data (Fig. 11a), accounting for 42% and 37%, respectively. Higher modes of surface waves are known to be dominant at sites where large stiffness contrasts and/or velocity reversals exist (O'Neil and Toshifumi, 2005). Clearly, the fundamental-mode energy dominates the low-frequency range (< 28 Hz) while the first-higher mode energy is dominant in the high-frequency range (≥ 28 Hz). Therefore, dispersion curves picked based on surface-wave energy in general are not exclusively the fundamental mode of surface waves resulting in reduced precision and reliability of inverted results. In extreme cases completely erroneous inverted results occurred (Xia *et al.*, 2003; Luo *et al.*, 2007).

We selected fundamental mode in the *f-v* domain (Fig. 11b) and applied the forward Radon transform to generate data in the *t-x* domain that contains only fundamental-mode Rayleigh waves (Fig. 12a). Thirty-five dispersion curves were calculated by a pair of consecutive traces within the mode-separated shot gather using formula (4). Phase-velocity section is generated by interpolation of 35 dispersion curves (Fig. 12b).

The phase velocity section (Fig. 12b) reveals a slope change along the survey direction. According to one-half-wavelength estimations (Sanchez-Salinero *et al.*, 1987) and different wavelengths carrying geological information at different depths (Babushka and Cara, 1991), we can roughly interpret the phase-velocity section as a slope variation

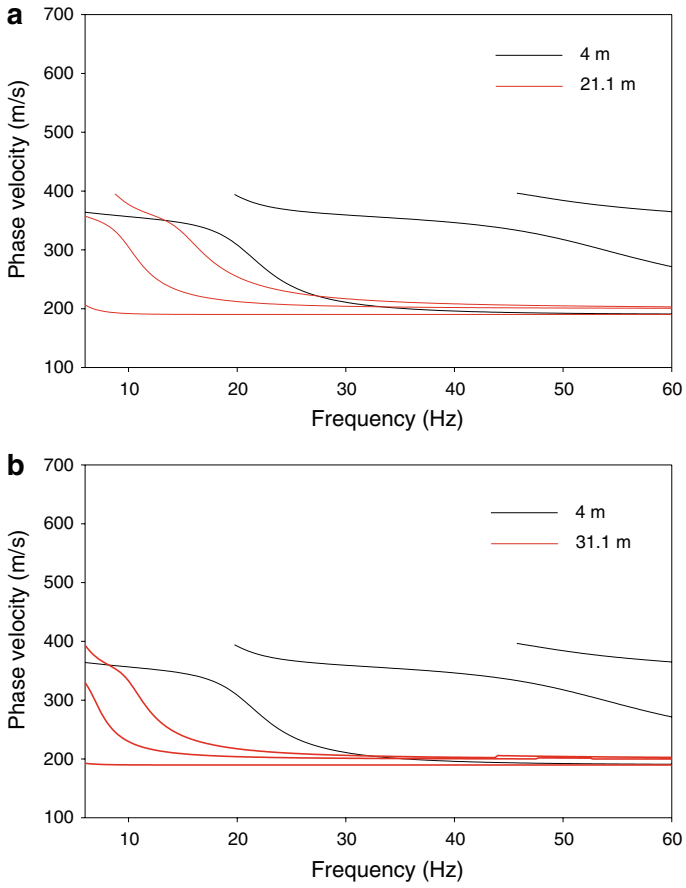

Figure 10

(a) The fundamental-, first-, and second-mode theoretical dispersion curves due to a 20-degree slope model calculated by the Knopoff method (SCHWAB and KNOPOFF, 1972). (b) The fundamental-, first-, and second-mode theoretical dispersion curves due to a 30-degree slope model calculated by the Knopoff method (SCHWAB and KNOPOFF, 1972).

from about 2.5 m to 5.5 m, deeming 230 m/s phase velocity as the threshold value between the dipping layer and the half space.

We also used the seismic-refraction method to image the bedrock for comparison with the results from the surface-wave method (Fig. 12b). Four shot gathers and corresponding reciprocal traveltime are shown in Figures 13a and 13b. The depth section (Fig. 13c) was calculated with the reciprocal traveltime curves (PALMER, 1981). We notice that (1) depth section reveals a slope interface with depth from about 3 m to 6 m; and (2) the phase velocity section (Fig. 12b) shows a similar result with the depth section (Fig. 13c) in the horizontal locations of 0–17.5 m with a depth range from 3 m to 5.5 m. The results of the real-world example further demonstrate that a dipping velocity

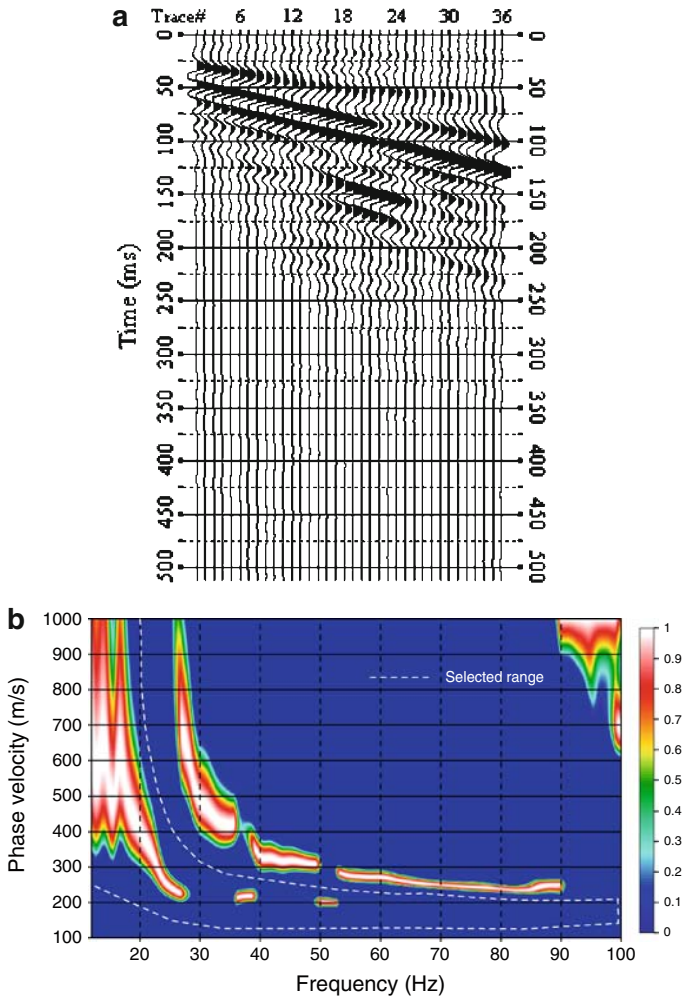

Figure 11
(a) 36-channel surface-wave data acquired at the campus of China University of Geosciences, Wuhan, China, during the spring of 2007. (b) A dispersive image in the *f-v* domain calculated by high-resolution LRT and the selected fundamental mode in dash lines.

interface with a slope smaller than 15 degrees can be successfully mapped by mode-separated phase velocities by high-resolution LRT.

5. Discussion and Conclusions

The main objective of the present work is to assess limitations of the MASW method. We used synthetic models containing a dipping layer with a slope of 5, 10, 15, 20, or 30

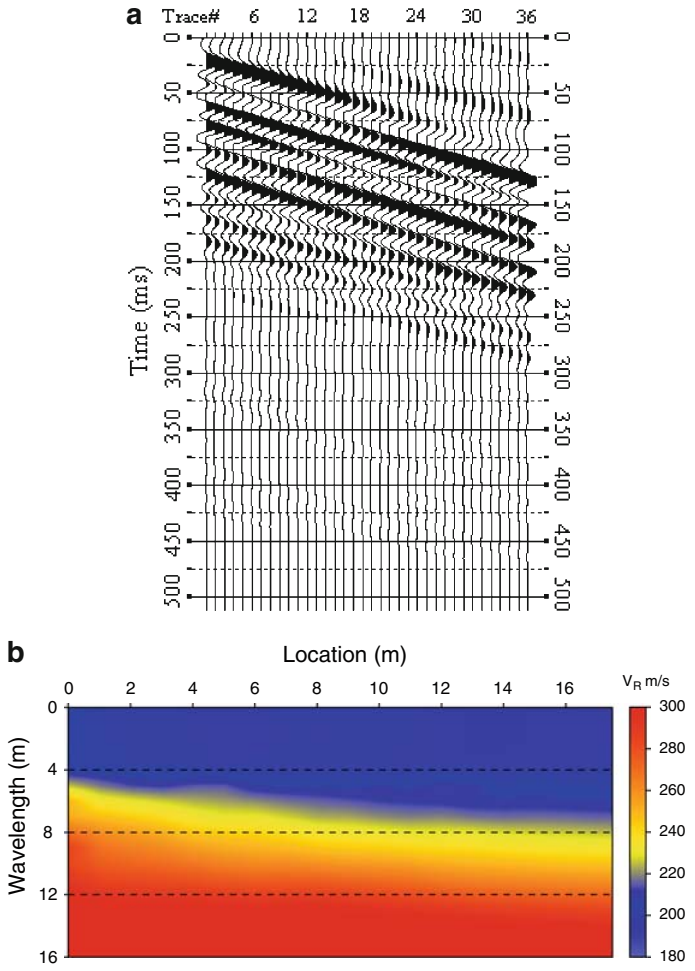

Figure 12
(a) The regenerated fundamental-mode shot gather. (b) Phase velocity section generated by interpolation of a series of dispersion curves calculated by a pair of consecutive traces in the regenerated fundamental-mode shot gather (a).

degrees and a real-world example to assess the ability of using high-resolution LRT to image and separate fundamental-mode Rayleigh waves from raw surface-wave data and accuracy of dispersion curves generated by a pair of consecutive traces within the mode-separated shot gather.

Results of the slope models demonstrate that (1) if the dip angle is smaller than 15°, phase-velocity sections generated a pair of consecutive traces after mode separation possess less than 10% relative errors compared with analytical results. As a rule of thumb, therefore, inverted S-wave velocities will possess over 90% accuracy (Xia *et al.*,

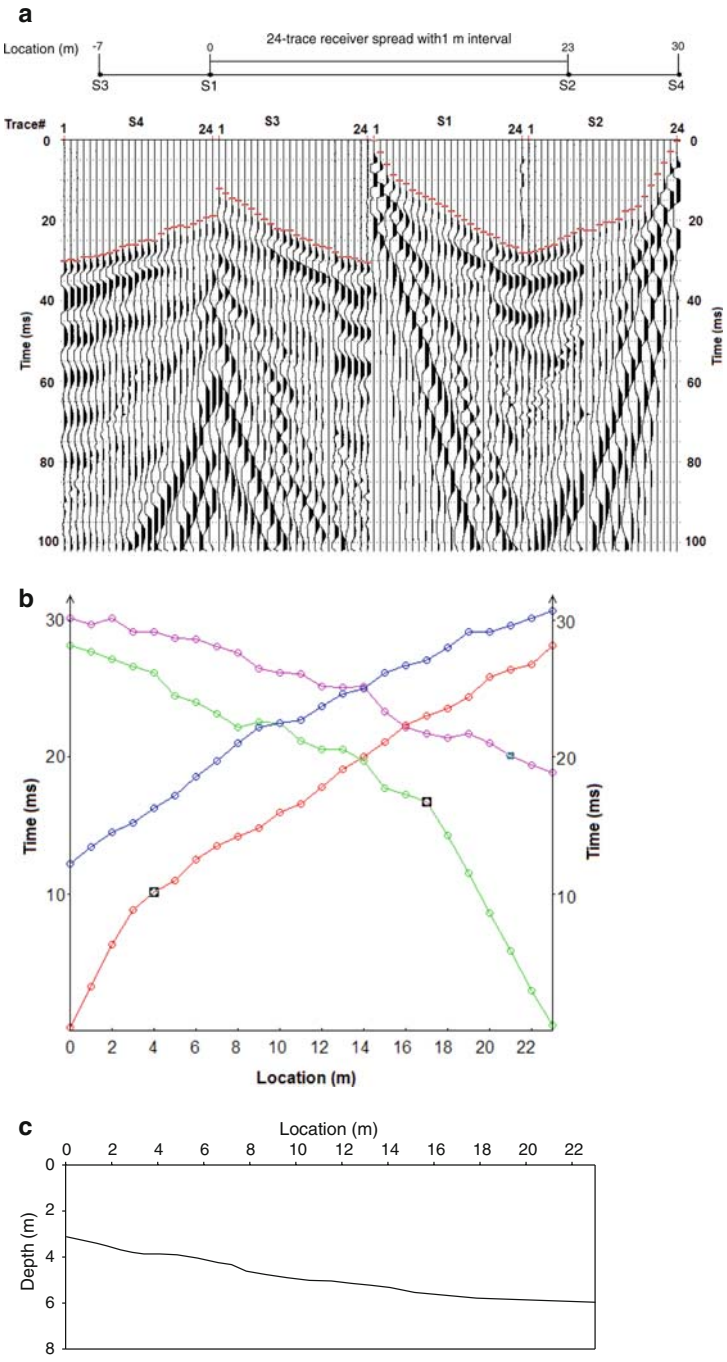

Figure 13
(a) Four seismic-refraction shot gathers. (b) Reciprocal traveltime curves. (c) Depth section calculated by a refraction method (PALMER, 1981).

1999, 2002a); and (2) if the dip angle is larger than 15°, Rayleigh-wave modes interfere with each other in the *f-v* domain making it impossible to separate fundamental-mode Rayleigh waves from surface-wave data by high-resolution LRT. Therefore, we are unable to calculate high-accuracy dispersion curves with a pair of consecutive traces. Results of a real-world example demonstrate that the phase-velocity section (Fig. 12b) clearly reveals a slope change along the survey direction. Compared with results generated by the seismic refraction method, phase velocity section (Fig. 12b) shows a similar result with the depth section (Fig. 13c) in the horizontal locations of 0–17.5 m with the depth ranges from 3 m to 5.5 m. The results of the real-world example further indicate that, if the slope degree is smaller than 15°, we can use high-resolution LRT to image and separate fundamental mode Rayleigh waves from raw surface-wave data and calculate dispersion curves using a pair of consecutive traces within a mode-separated shot gather. One also notices that the signal-to-noise ratio will greatly affect the accuracy of calculated dispersion curves. Luo *et al.* (2008a) provided a guideline for defining a trade-off between a receiver spacing and accuracy of calculated dispersion curves.

Properly separating fundamental-mode Rayleigh waves from raw surface-wave data is a key step for high horizontal-resolution 2D S-wave velocity mapping by calculating dispersion curves with a pair of consecutive traces. Luo *et al.* (in review) presented several guidelines for fundamental-mode separation from raw surface-wave data. However, great effort should be spent on integrating all seismic and geological information, such as subsurface geological structure, drilling data, local-outcrop analysis, body waves, and so on, to properly carry out mode separation.

Acknowledgments

The first author appreciates the Kansas Geological Survey, the University of Kansas, for providing opportunities in surface-wave research and the China Scholarship Council for the financial support to conduct this study. The authors wish to thank Öz Yilmaz for helpful discussion and suggestions on plan-wave decomposition and the Radon transform. We are particularly grateful to Mauricio D. Sacchi, Daniel Trad, and Wang Juefu for their constructive advice in high-resolution LRT programming. The authors thank Marla Adkins-Heljeson of the Kansas Geological Survey for editing the manuscript.

References

Babuska, V. and Cara, M., *Seismic Anisotropy in the Earth* (Academic Publishers 1991).

Bodet, L., Wijk, K.V., Bitri, A., Abraham, O., and Côte, P. (2005), *Surface-wave inversion limitations from laser-doppler physical modeling*, J. Environm. Engin. Geophys. *10*(2), 151–162.

Calderón-Macías, C. and Luke, B. (2007), *Improved parameterization to invert Rayleigh-wave data for shallow profiles containing stiff inclusions*, Geophys. *72*(1), U1–U10.

Ethan, J.N. and Matthias, G.I. (2006), *Amplitude preservation of Radon-based multiple-removal filters*, Geophys. *71*(5), V123–V126.

GUO, T. and LIU, L. (1999), *Non-intrusive evaluation of submarine tunnel foundation using dynamic high-frequency surface wave prospecting*, Proc. Symp. on the Application of Geophysics to Engineering and Environmental Problems (Environmental and Engineering Geophysics Society), Oakland, CA. 67–74.

HAYASHI, K. and SUZUKI, H. (2004), *CMP cross-correlation analysis of multi-channel surface-wave data*, Exploration Geophys. *35*, 7–13.

KUO, J.T. and THOMPSON, G.A. (1963), *Model studies on the effect of a sloping interface on Rayleigh waves*, J. Geophys. Res. *68*(22), 6187–6197.

LIU, J.P., HOU, W. and XU, S. (2003), *Adjacent-channel transient Rayleigh wave method and its application in compression strength test of water-tight wall, Yangtze River* (in Chinese with English abstract). *34*, 53–56.

LUO, Y., XIA, J., MILLER, R.D., XU, Y., LIU, J., and LIU, Q. (in review), *Rayleigh-wave mode separation by high-resolution linear Radon transform*, Geophys. J. Internat.

LUO, Y., XIA, J., LIU, J., XU, Y., and LIU, Q. (2008a), *Generation of a pseudo-2D shear – wave velocity section by inversion of a series of ID dispersion curves*, J. Appl. Geophys. *64*(3), 115–124.

LUO, Y., XIA, J., LIU, J., XU, Y., and LIU, Q. (2008b), *Research on the MASW middle-of-the- spread-results assumption*, Soil Dyn. Earthq. Engin. DOI:10.1016/ j.soildyn.2008.01.009.

LUO, Y., XIA, J., MILLER, R.D., XU, Y., LIU, J., and LIU, Q. (2008c), *Rayleigh-wave dispersive energy imaging by high-resolution linear Radon transform*, Pure Appl. Geophys. *165*, 903–922.

LUO, Y., XIA, J., LIU, J., LIU, Q., and XU, S. (2007), *Joint inversion of high-frequency surface waves with fundamental and higher modes*, J. Appl. Geophys. *62*, 375–384.

MCMECHAN, G.A. and YEDLIN, M.J. (1981), *Analysis of dispersive waves by wave field transformation*, Geophys. *46*, 869–874.

MILLER, R.D., XIA, J., PARK, C.B., and IVANOV, J. (1999), *Multichannel analysis of surface waves to map bedrock*, The Leading Edge *18*, 1392–1396.

O'NEILL, A. and TOSHIFUMI, M. (2005), *Dominant higher surface-wave modes and possible inversion pitfalls*, J. Environm. Engin. Geophys. *10*(2), 185–201.

PALMER, D. (1981), *An introduction to the generalized reciprocal method of seismic refraction interpretation*, Geophys. *46*(11), 1508–1518.

PARK, C.B., MILLER, R.D., and XIA, J. (1998), *Imaging dispersion curves of surface waves on multi-channel record*, Technical Program with Biographies SEG, 68th Annual Meeting, New Orleans, LA. 1377–1380.

PARK, C.B., MILLER, R.D., and XIA, J. (1999), *Multi-channel analysis of surface waves (MASW),* Geophys. *64*, 800–808.

PARK, C.B. (2005), *MASW horizontal resolution in 2D shear-velocity (Vs) mapping*, Kansas Geological Survey Open-file Report 2005–4.

SACCHI, M. and ULRYCH, T. (1995), *High resolution velocity gathers and offset space reconstruction*, Geophys. *60*, 1169–1177.

SACCHI, M. and PORSANI, M. (1999), *Fast high resolution parabolic RT*, 69th Annual International Meeting, Society of Exploration Geophysicists, Expanded Abstracts. 1477–1480.

SANCHEZ-SALINERO, I., ROESSET, J.M., SHAO, K.Y., STOKOE II, K.H., and RIX, G.J. (1987), *Analytical evaluation of variables affecting surface wave testing of pavements*, Transportation Res. Record No. 1136, 86–95.

SCHONEWILLE, M.A. and DUIJNDAM, A.J.W. (2001), *Parabolic Radon transform, sampling and efficiency*, Geophys. *66*(2), 667–678.

SCHWAB, F.A. and KNOPOFF, L., *Fast surface wave and free mode computations, In Methods in Computational Physics* (ed. B.A. Bolt), (Academic Press, New York, (1972)) pp. 87–180.

SONG, Y.Y., CASTAGNA, J.P., BLACK, R.A., and KNAPP, R.W. (1989), *Sensitivity of near-surface shear-wave velocity determination from Rayleigh and Love waves*, Technical Program with Biographies, SEG, 59th Annual Meeting, Dallas, TX, 509–512.

TRAD, D., ULRYCH, T., and SACCHI, M. (2002), *Accurate interpolation with high-resolution time-variant radon transforms*, Geophys. *67*(2), 644–656.

TRAD, D., ULRYCH, T., and SACCHI, M. (2003), *Latest views of the sparse Radon transform*, Geophys. *68*, 386–399.

XIA, J., MILLER, R.D. and PARK, C.B. (1999), *Estimation of near-surface shear-wave velocity by inversion of Rayleigh wave*, Geophys. *64*, 691–700.

XIA, J., MILLER, R.D., PARK, C.B., HUNTER, J.A., HARRIS, J.B., and IVANOV, J. (2002a), *Comparing shear-wave velocity profiles from multichannel analysis of surface wave with borehole measurements*, Soil Dyna. Earthq. Engin. *22*(3), 181–190.

XIA, J., MILLER, R.D., PARK, C.B., WIGHTMAN, E., and NIGBOR, R. (2002b), *A pitfall in shallow shear-wave refraction surveying,* J. Appl. Geophys. *51*(1), 1–9.

XIA, J., MILLER, R.D., PARK, C.B., and TIAN, G. (2003), *Inversion of high frequency surface waves with fundamental and higher modes*, J. Appl. Geophys. *52*(1), 45–57.

XIA, J., CHEN, C., TIAN, G., MILLER, R.D., and IVANOV, J. (2005), *Resolution of high-frequency Rayleigh-wave data*, J. Environm. Engin. Geophys. *10*(2), 99–110.

XIA, J., XU, Y., MILLER, R.D., and CHEN, C. (2006), *Estimation of elastic moduli in a compressible Gibson half-space by inverting Rayleigh wave phase velocity*, Surveys in Geophys. *27*(1), 1–17.

XIA, J., XU, Y., and MILLER, R.D. (2007a), *Generating image of dispersive energy by frequency decomposition and slant stacking*, Pure Appl. Geophys. *164*(5), 941–956.

XIA, J., NYQUIST, J.E., XU, Y., ROTH, M.J.S., and MILLER, R.D. (2007b), *Feasibility of detecting near-surface feature with Rayleigh-wave diffraction*, J. Appl. Geophys. *62*(3), 244–253.

XU, Y., XIA, J., and MILLER, R.D. (2007), *Numerical investigation of implementation of air/earth boundary by acoustic/elastic boundary approach*, Geophys. *72*, SM147-SM153.

YILMAZ, Ö. (1987), *Seismic data processing*, Society of Exploration Geophysicists, Tulsa, OK.

(Received September 15, 2007, revised September 16, 2008)
Published Online First: February 28, 2009